


 CrossMark  
 click for updates

Cite this: DOI: 10.1039/c6ce00878j

## *In situ* asymmetric island sidewall growth of high-quality semipolar (11 $\bar{2}$ 2) GaN on *m*-plane sapphire

 Zhengyuan Wu,<sup>a</sup> Xiyang Shen,<sup>a</sup> Chuan Liu,<sup>b</sup> Kongyi Li,<sup>a</sup> Wenzhong Shen,<sup>c</sup>  
 Junyong Kang<sup>a</sup> and Zhilai Fang<sup>\*a</sup>

*In situ* asymmetric island sidewall growth (AISG) was developed to enhance Ga-face facet growth and improve the crystalline quality of (11 $\bar{2}$ 2) GaN epilayers on *m*-plane sapphire substrates. In the early growth stage island shaping and sidewall faceting were distinct and controlled by growth design. Using *in situ* AISG, {0002} instead of { $\bar{1}$ 103} sidewall facets were formed on the Ga-rich island surface, which eliminated formation of a { $\bar{1}$ 103} phase during subsequent layer growth of semipolar GaN. Enhanced Ga-face sidewall facet growth led to +*c* regions overlapping –*c* regions, which reduced defect density. Pure semipolar (11 $\bar{2}$ 2) epilayers with a reduced surface striation density and a basal-plane stacking fault density of  $8 \times 10^3 \text{ cm}^{-2}$  were obtained. The observation of a narrow  $E_2^H$  peak and an intense  $E_1(\text{LO})$  peak in Raman spectra indicates that almost strain-free high-quality semipolar (11 $\bar{2}$ 2) GaN films were achieved. The photoluminescence emission intensity from the (11 $\bar{2}$ 2) GaN film prepared by *in situ* AISG was dominated by band-edge emission and enhanced  $\sim 4$  times more than that from conventional (11 $\bar{2}$ 2) GaN.

 Received 16th April 2016,  
 Accepted 3rd June 2016

DOI: 10.1039/c6ce00878j

www.rsc.org/crystengcomm

### Introduction

Growth and design of group-III nitride semiconductor heterostructures on semipolar planes have attracted intense research interest due to the reduction of the internal electric field inherently existing in polar III-nitrides growing along the *c* axis.<sup>1–7</sup> In comparison with nonpolar GaN, semipolar GaN grown on (11 $\bar{2}$ 2) and (20 $\bar{2}$ 1) atomic planes has the merits of a high indium incorporation efficiency<sup>8</sup> and a wide growth window.<sup>9,10</sup> (11 $\bar{2}$ 2) semipolar GaN is of a nearly free electric field and thus preferred as a growth template of long-wavelength GaN-based optoelectronic devices. Owing to a lack of large-sized and low-priced GaN substrates, semipolar (11 $\bar{2}$ 2) III-nitrides are usually grown on heterosubstrates.<sup>11–14</sup> Unfortunately, semipolar (11 $\bar{2}$ 2) GaN heteroepitaxial films usually have high-density structural defects and rough surfaces, which have become a big obstacle when fabricating high-performance devices.<sup>14–16</sup> Various methods such as two-step growth, SiN<sub>x</sub> or ScN or superlattice interlayering, chemical etching, and epitaxial lateral overgrowth (ELO) have been developed to reduce the density of threading dislocation (TD),

partial dislocation (PD), and stacking faults (SFs) in semipolar (11 $\bar{2}$ 2) GaN.<sup>17–23</sup> In conventional ELO the SF density was significantly reduced in +*c* wings but remained very high in –*c* wings and windows.<sup>22–26</sup> This indicates that enhanced Ga-face sidewall facet (also referred as +*c* plane) growth, which increases the area of the +*c* region, may improve the crystalline quality of semipolar (11 $\bar{2}$ 2) GaN films. However, conventional ELO requires a complicated *ex situ* lithography process with a risk of contamination. Furthermore, thick GaN layers have to be grown for full coalescence and surface smoothing. Conventional ELO is generally time-consuming and expensive though the quality of ELO-grown GaN is highly attractive.

Heteroepitaxy usually leads to the formation of three-dimensional islands in early growth stages, which has a significant influence on film qualities. For instance, high-density defects are usually formed at the coalescence boundary of adjacent misoriented islands.<sup>27–29</sup> Therefore, the monitoring of island shaping and shape variation in the early growth stages of GaN heteroepitaxy is crucial for the growth of high-quality GaN films.<sup>30–34</sup> In this study, different from conventional ELO, *in situ* asymmetric island sidewall growth (AISG) for faster and more uniform coalescence of neighboring islands was developed in order to enhance Ga-face island sidewall facet growth and to improve the crystalline quality and optical properties of the semipolar (11 $\bar{2}$ 2) GaN epilayers without the *ex situ* lithography process. We find that by *in situ* AISG the heteroepitaxially grown semipolar GaN films are of (11 $\bar{2}$ 2) single phase, reduced SF density, and enhanced band-edge emission.

<sup>a</sup> Collaborative Innovation Center for Optoelectronic Semiconductors and Efficient Devices, Department of Physics, Xiamen University, Xiamen 361005, China.  
E-mail: zhilaifang@hotmail.com

<sup>b</sup> College of Chemistry and Chemical Engineering, Xiamen University, Xiamen 361005, People's Republic of China

<sup>c</sup> Key Laboratory of Artificial Structures and Quantum Control (Ministry of Education), Department of Physics, Shanghai Jiao Tong University, Shanghai 200240, China

## Experimental

The heteroepitaxy of semipolar GaN films on (1100) *m*-plane sapphire substrates was carried out in a Thomas Swan metalorganic chemical vapor deposition system. Trimethylgallium (TMGa) and high-purity ammonia were used as the source precursors, and hydrogen as the carrier gas. The sapphire substrates were cleaned at 1060 °C and 100 Torr for 10 min in a H<sub>2</sub> ambient atmosphere followed by nitridation at 570 °C for 6 min. A low-temperature GaN nucleation layer (NL, ~30 nm thick) was grown at 550 °C and 500 Torr for 120 s followed by a high-temperature annealing process at 1030 °C. The GaN epilayers at different growth stages were prepared by varying the growth time, temperature, pressure, and NH<sub>3</sub>/TMGa ratio for the investigation of growth behavior. High reactor pressure (250 Torr) was employed for the formation of energetically more stable island sidewall facets at the initial growth stages and then was gradually decreased to 120 Torr for island coarsening and coalescence. The reactor pressure was further decreased and finally kept at 50 Torr for the lateral growth of semipolar GaN films with a smooth surface. Sample “A1” was prepared under conventional growth conditions (at 1030 °C and 250 Torr for 400 s) as a control sample of GaN islands on the NL. After that further GaN growth was carried out at 120 Torr for 800 s on sample “A1”. Sample “B1” was prepared by intentionally prolonging the island growth for 1000 s with a low NH<sub>3</sub>/TMGa ratio of 1100 at 1030 °C. Growth with a low NH<sub>3</sub>/TMGa ratio and at high growth temperature in the initial growth stage is expected to enhance Ga adatom diffusion and Ga-polar sidewall facet growth, and suppress the formation of stable N-polar sidewall facets. By the proposed *in situ* AISG for sample “B1”, the island sidewall facets are expected to gradually change from N-polar to Ga-polar; meanwhile, during island coalescence the *-c* regions of one island would be covered with high-quality *+c* regions of neighboring islands. Samples “A2” and “B2” were prepared by a subsequent layer growth of ~2.5 μm thick GaN on samples “A1” and “B1” with a high NH<sub>3</sub>/TMGa ratio of 2176 and low reactor pressure of 50 Torr.

The surface morphologies of the semipolar GaN epilayers were investigated by atomic force microscopy (AFM, SII SPA400) and scanning electron microscopy (SEM, Hitachi-S4800). The surface chemical compositions were analyzed by X-ray photoelectron spectroscopy (XPS, PHI Quantum2000) with an Al K<sub>α</sub> X-ray excitation source (*hν* = 1486.6 eV). Spatially-resolved surface chemical compositions were characterized by elemental mapping using a SEM installed with an energy dispersive spectroscope (EDS, SU70). The SEM-EDS operating voltage is 10–20 kV and the collection time is 40 s. Different areas have been measured for consistency. X-ray diffraction (XRD, PHILIPS X'Pert PRO) and Raman spectroscopy (RAMAN-11) were used to qualitatively analyze the crystalline quality of semipolar GaN. The luminescence properties of the semipolar GaN were investigated by micro-photoluminescence (PL) excited by a 325 nm He–Cd laser and spatially-resolved cathodoluminescence (CL, Gatan

MonoCL3+) at room temperature (300 K). An electron acceleration voltage of 5 kV and beam current of less than 20 nA were employed to avoid radiation damage during the SEM-CL measurements. The microstructure of sample “B2” was investigated by transmission electron microscopy (TEM, JEM2100) using an accelerating voltage of 200 kV.

## Results and discussion

In the early growth stage under high reactor pressure, adatom diffusion is limited and plays an important role in island shaping and shape variation.<sup>30–34</sup> Energetically more stable island sidewall facets of either Ga-polarity or N-polarity would be formed. Fig. 1 shows a schematic diagram of atomic structures for the {1122}, {1103}, and {1011} atomic planes (side view). The {0002} atomic plane is also shown for reference. Apparently, as confirmed by convergent beam electron diffraction,<sup>13,14</sup> the {1103} and {1011} atomic planes are of N-polarity (N-face) whereas the {0002} and {1122} atomic planes are of Ga-polarity (Ga-face). It has been reported that the N-polar surface is energetically more stable at low growth temperature with a high NH<sub>3</sub>/TMGa ratio and becomes unstable at high temperature with a low NH<sub>3</sub>/TMGa ratio.<sup>31</sup> This means that the island shaping and shape variation (*e.g.* formation of specific smooth sidewall facets, variation of island sidewall facets from N-polar to Ga-polar, *etc.*) may be well controlled by an appropriate growth design. In the following we present the studies on island shaping, shape variations, island coarsening and coalescence, and their influences on the growth of high-quality semipolar GaN films by *in situ* AISG.

Fig. 2 shows the XPS spectra of the Ga3d<sub>5/2</sub> and N1s photoelectron peaks from samples “A1” and “B1”. The XPS spectra were referenced to the XPS data book with the C1s peak fixed at 284.8 eV.<sup>35</sup> In the XPS spectra of the N1s photoelectron peak strong Ga Auger signals were also observed. The average gallium to nitrogen ratio ( $X_{\text{Ga/N}}^S$ ) can be estimated by the integrated intensity ratio of deconvoluted XPS components calibrated by the sensitivity factors. Based on

$$X_{\text{Ga/N}}^S = \frac{(I_{3d5/2})/(F_{3d5/2})}{(I_{N1s})/(F_{N1s})}, \text{ where } S \text{ denotes the sample name, } I$$

the integrated intensity and *F* the sensitivity factor ( $F_{\text{Ga}3d5/2} = 0.438$  and  $F_{\text{N}1s} = 0.499$ ), we get  $X_{\text{Ga/N}}^{\text{A1}} \approx 1.00$  and  $X_{\text{Ga/N}}^{\text{B1}} \approx 1.07$  for samples “A1” and “B1”, respectively. In comparison with sample “A1”, the slight increase of the Ga/N ratio for sample “B1” indicates the formation of a Ga-rich surface by *in situ* AISG under high-pressure and Ga-rich growth conditions. On the Ga-rich surface the N-polar sidewall facet would become unstable and Ga-face facet growth would be enhanced.<sup>36</sup>

Fig. 3a shows a schematic diagram of (1122) GaN on the (1100) *m*-plane sapphire substrates. The epitaxial relationship between GaN and sapphire is identified as  $[1122]_{\text{GaN}} \parallel [1100]_{\text{sapphire}}$ ,  $[\bar{1}\bar{1}23]_{\text{GaN}} \parallel [0001]_{\text{sapphire}}$ , and  $[1100]_{\text{GaN}} \parallel [11\bar{2}0]_{\text{sapphire}}$ . Fig. 3b shows the SEM image of sample “A1”. High-density partially coalesced trapezoidal faceted

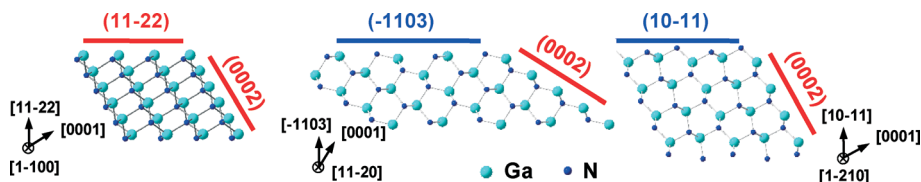


Fig. 1 Schematic diagram of atomic structures for the  $\{11\bar{2}2\}$ ,  $\{\bar{1}103\}$ , and  $\{10\bar{1}1\}$  atomic planes (side view).

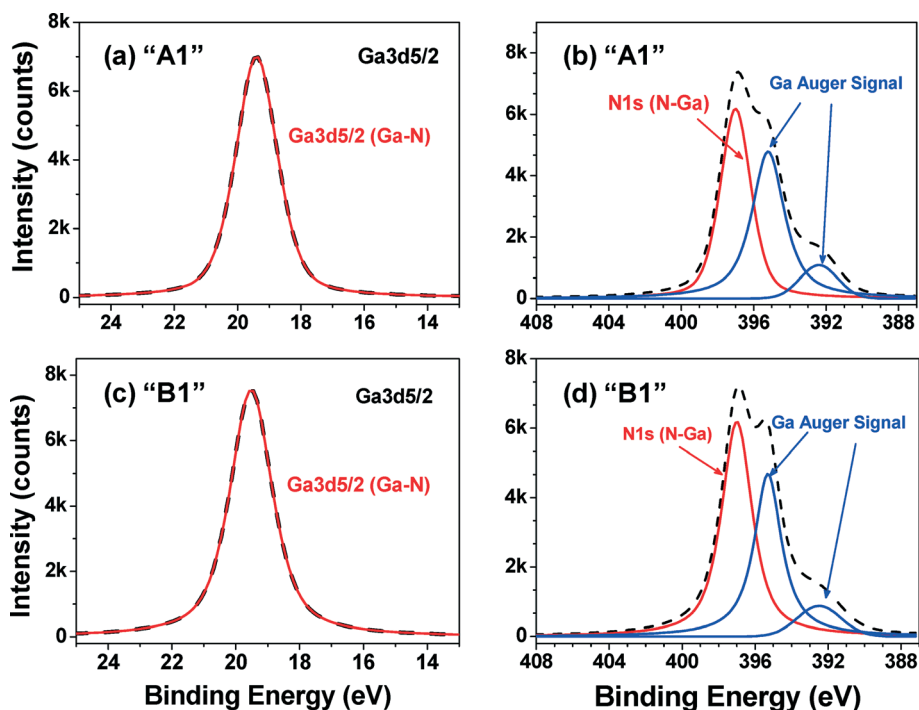


Fig. 2 XPS spectra of (a) Ga3d5/2 and (b) N1s photoelectron peaks of sample "A1". XPS spectra of (c) Ga3d5/2 and (d) N1s photoelectron peaks of sample "B1". In the figure, the fitted peaks of 19.5 eV and 397.0 eV correspond to Ga3d5/2 (Ga-N) and N1s (N-Ga), respectively.

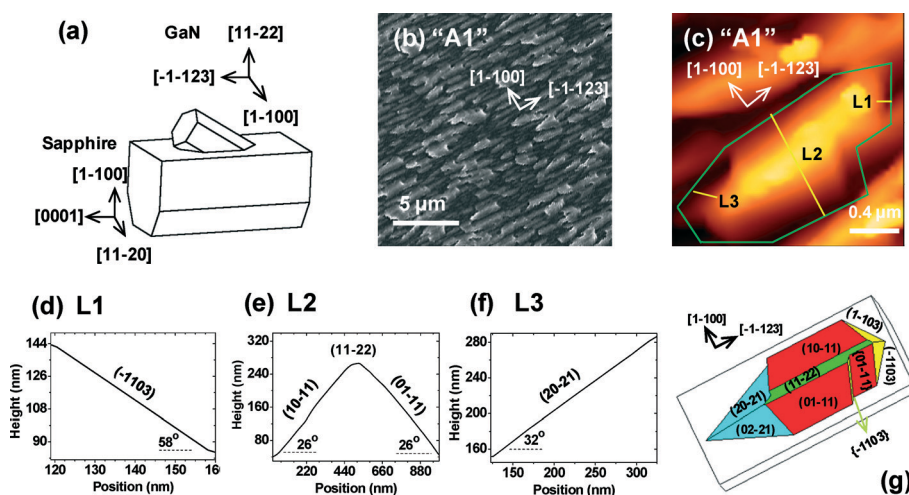


Fig. 3 (a) Schematic diagram of semipolar  $\{11\bar{2}2\}$  GaN on the  $\{1\bar{1}00\}$  *m*-sapphire substrates showing the epitaxial relationship between GaN and sapphire. (b) SEM image of the surface morphology of sample "A1". (c) AFM image of typical GaN islands of sample "A1". Line profiles (d) "L1", (e) "L2", and (f) "L3" crossing over the typical sidewall facets of the island marked by green lines. (g) A geometrical model of the island showing the presence of island sidewall facets of various polar angles.

islands with a ridge-like top and arrowhead to  $[\bar{1}\bar{1}23]$  were observed. To further investigate the three-dimensional structure of the GaN islands, the surface morphology was also investigated by AFM. The typical island shape of sample "A1" is shown in Fig. 3c. Line profiles "L1", "L2", and "L3" crossing over the typical sidewall facets of the island marked by green lines were drawn and shown in Fig. 3d–f. The specific polar angles of the sidewall facets referring to the  $(11\bar{2}2)$  basal plane are measured to be  $58^\circ$ ,  $26^\circ$ ,  $0^\circ$ , and  $32^\circ$ , respectively, indicating the presence of  $\{\bar{1}103\}$ ,  $\{10\bar{1}1\}$ ,  $\{11\bar{2}2\}$ , and  $\{20\bar{2}1\}$  sidewall facets on the island surface. Based on the AFM images, line profiles, and SHAPE software, we sketch in Fig. 3g the geometrical model of the island with various island sidewall facets formed under conventional growth conditions.

Fig. 4a and b shows the SEM and AFM images of sample "B1". The islands are mesa-like and mostly coalesced. A geometrical model for the coalesced islands marked by red lines is sketched in Fig. 4c. Interestingly, in comparison with sample "A1",  $\{0002\}$  instead of  $\{\bar{1}103\}$  sidewall facets were observed on the islands of sample "B1". Under the *in situ* AISG growth conditions for sample "B1" the Ga-polar  $\{0002\}$  sidewall facets are energetically more stable than the N-polar  $\{\bar{1}103\}$  sidewall facets, leading to a gradual change of N-polar to Ga-polar sidewall facets, which is consistent with the discussions for Fig. 1 and the XPS analysis in Fig. 2. Furthermore, the  $\{\bar{1}103\}$  atomic planes have a higher dangling bond density ( $14.2 \text{ nm}^{-2}$ ) than that of the  $\{0002\}$  planes ( $11.4 \text{ nm}^{-2}$ ) and thus would grow faster and eventually disappear.<sup>31</sup> The Ga-face facet growth was enhanced and the  $\{\bar{1}103\}$  facet growth was suppressed, which would eliminate the formation of the  $\{\bar{1}103\}$  phase during the subsequent layer growth of semipolar GaN. Fig. 4d shows a schematic diagram of the is-

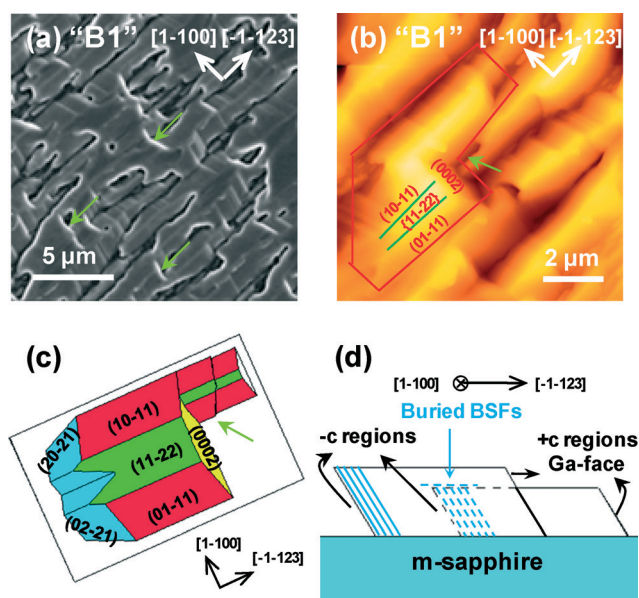


Fig. 4 (a) SEM and (b) AFM images of sample "B1". (c) A geometrical model of the coalesced island marked by red lines. (d) Schematic diagram of island coalescence along  $[\bar{1}\bar{1}23]$  showing the covering of the  $-c$  region of one island by the  $+c$  region of an adjacent island.

land coalescence process. As indicated by the green arrows, the  $+c$  region of one island overlaps the  $-c$  region of a neighboring island during coalescence along  $[\bar{1}\bar{1}23]$  due to the enhanced Ga-face facet growth. As a result, high-density basal plane SFs (BSFs) usually generated in the  $-c$  regions are blocked by the  $+c$  regions on top.

Fig. 5 shows the SEM image and EDS elemental mappings for Ga  $K_{\alpha 1}$  (red) and N  $K_{\alpha 1}$  (green) over the same area of sample "A1". Yellow dashed circles are marked in the same region of one typical island side and white dashed circles are marked in the same region of the other island side. In Fig. 5b and c the intensities (counts) within the yellow circles of the Ga  $K_{\alpha 1}$  and N  $K_{\alpha 1}$  elemental maps are stronger than those within the white circles. Fig. 5d shows the EDS line profiles (red curve for Ga and green for N) from the yellow circled region to the white circled region of the typical island along  $[\bar{1}\bar{1}23]$  as indicated by the red arrow. The line profiles are fitted and shown as black curves. The tendency of the Ga/N intensity (without calibration) is roughly estimated from the black fitted curves and drawn as a line of blue circles. The tendency curve shows a decrease of Ga/N along  $[\bar{1}\bar{1}23]$ . We denote the yellow circled region as the  $+c$  region and the white circled region as the  $-c$  region of the island accordingly.

Fig. 6 shows the SEM image and EDS elemental mappings for Ga  $K_{\alpha 1}$  (red) and N  $K_{\alpha 1}$  (green) over the same area of sample "B1". Typically for the island coalescence regions (e.g., green circled), the Ga elemental distributions show intensity fluctuation whereas the N elemental distributions are relatively uniform, indicating the presence of partial overlapping of the  $+c$  and  $-c$  regions during island coalescence of neighboring islands. Fig. 6d shows the EDS line profiles crossing over the coalescence regions of neighboring islands along  $[\bar{1}\bar{1}23]$  as indicated by the red arrow. The tendency of the Ga/N

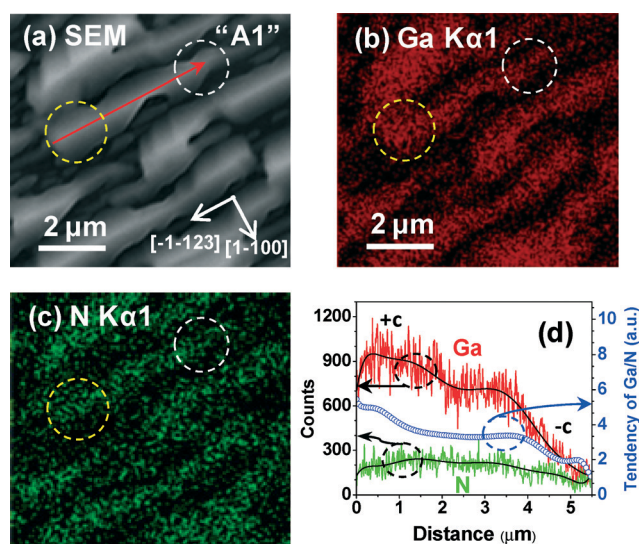


Fig. 5 SEM image (a) and EDS elemental mappings for (b) Ga  $K_{\alpha 1}$  (red) and (c) N  $K_{\alpha 1}$  (green) over the same area of sample "A1". (d) EDS line scan along  $[\bar{1}\bar{1}23]$  as indicated by the red arrow.

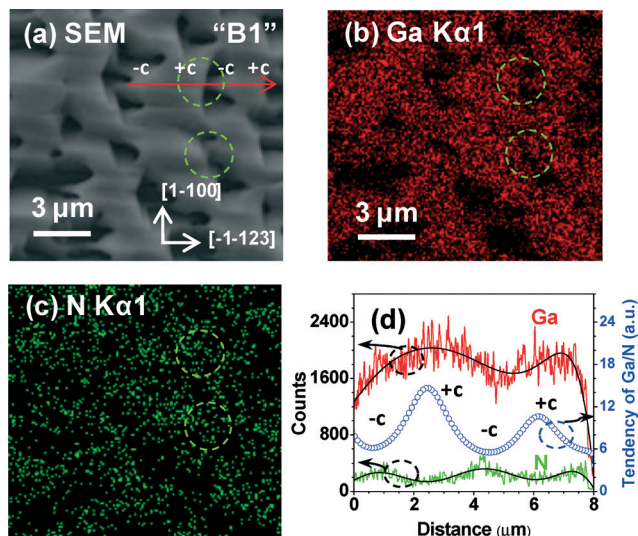


Fig. 6 SEM image (a) and EDS elemental mappings for (b) Ga  $K_{\alpha 1}$  (red) and (c) N  $K_{\alpha 1}$  (green) over the same area of sample "B1". (d) EDS line scan along  $[1\bar{1}2\bar{3}]$  as indicated by the red arrow.

N intensity (without calibration) is roughly estimated from the fitted curves and drawn as a line of blue circles. The tendency curve shows a strong fluctuation of Ga/N with distinct peaks and dips corresponding to the  $+c$  regions and  $-c$  regions, respectively. The  $+c$  regions (Ga-face island sidewall facets) are obviously of large area (height and width), indicating enhanced Ga-face sidewall facet growth. This led to the  $+c$  region of one island overlapping the  $-c$  region of a neighboring island during island coalescence. Due to *in situ* AISG, enhanced Ga-face sidewall facet growth and the overlapping of the  $+c$  and  $-c$  regions between two neighboring islands in sample "B1" are much more effective than that in sample "A1" due to the formation of a Ga-rich surface (see Fig. 2) and the intentionally prolonged island growth with a low  $\text{NH}_3/\text{TMGa}$  ratio and high reactor pressure. The  $-c$  regions of high-density defects would be eventually covered by the high-quality  $+c$  regions, resulting in a significant reduction of BSF density in the semipolar  $(1\bar{1}\bar{2}\bar{2})$  GaN films.

Fig. 7 shows the SEM images of samples "A2" and "B2". The inset AFM images give a close view of the surface morphology. Typical striations were observed for both samples.

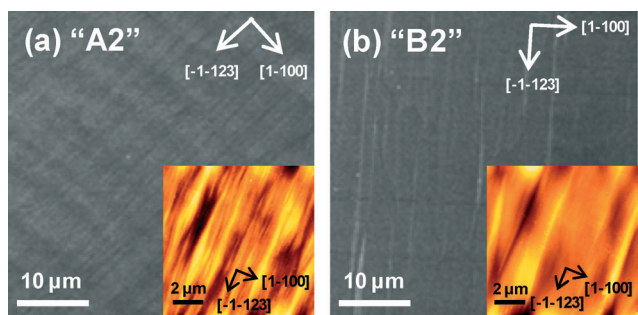


Fig. 7 SEM images of samples (a) "A2" and (b) "B2". The inset AFM images give a close view of the surface morphology.

The average striation density of sample "A2" was estimated to be  $\sim 0.46$  and  $0.16 \mu\text{m}^{-1}$  along  $[\bar{1}100]$  and  $[1\bar{1}\bar{2}\bar{3}]$ , respectively. The presence of high-density striations on the surface indicates growth anisotropy and high-density BSFs generated at the coalescence boundary of neighboring islands.<sup>14,20</sup> The average striation density of sample "B2" was estimated to be  $\sim 0.26$  and  $0.10 \mu\text{m}^{-1}$  along  $[\bar{1}100]$  and  $[1\bar{1}\bar{2}\bar{3}]$ , respectively. The decrease in striation density indicates the reduction of the BSF density in sample "B2".<sup>18,20</sup>

Fig. 8a shows the XRD  $\omega$ - $2\theta$  scans of samples "A2" and "B2". The simultaneous appearance of the primary  $(1\bar{1}\bar{2}\bar{2})$  peak at  $34.6^\circ$  and the secondary  $(10\bar{1}\bar{3})$  peak at  $32.3^\circ$  from sample "A2" indicates the presence of mixed phases. The integrated intensity ratio of  $(10\bar{1}\bar{3})$  GaN to  $(1\bar{1}\bar{2}\bar{2})$  GaN is  $\sim 4\%$ . Semipolar  $(10\bar{1}\bar{3})$  GaN has twinned crystallites and a rough surface, which is deleterious to the crystalline quality and device performance. The presence of the  $(10\bar{1}\bar{3})$  phase in sample "A2" is likely a consequence of GaN growth on the exposed  $(10\bar{1}\bar{3})$  island sidewall facets in sample "A1" (see Fig. 3). In comparison, for sample "B2" a single  $(1\bar{1}\bar{2}\bar{2})$  peak was observed indicating that pure semipolar  $(1\bar{1}\bar{2}\bar{2})$  GaN was obtained. The absence of the  $(10\bar{1}\bar{3})$  peak is consistent with the initial island sidewall faceting in sample "B1" (without formation of the  $\{10\bar{1}\bar{3}\}$  sidewalls by *in situ* AISG in the early growth stage).

Fig. 8b shows the XRD  $\omega$  scans of the  $(1\bar{1}\bar{2}\bar{2})$  peaks from samples "A2" and "B2". In previous studies, as far as we know, the full width at half maximum (FWHM) of the XRD peak for polar  $c$ -plane GaN was as small as 158 arcsec;<sup>37</sup> the FWHMs of the XRD peaks for nonpolar  $a$ -plane GaN on sapphire with ScN interlayers or on patterned sapphire substrate (PSS) were 300 arcsec;<sup>19,38</sup> the FWHM of the XRD peaks for nonpolar  $m$ -plane GaN on PSS was 490 arcsec.<sup>39</sup> In semipolar  $(1\bar{1}\bar{2}\bar{2})$  GaN, the XRD  $\omega$ -scan peak broadening with the incident beam aligned to the  $[\bar{1}\bar{1}\bar{2}\bar{3}]$  direction is usually correlated with the BSF and dislocation density.<sup>19</sup> It has been reported that an FWHM of 1400 arcsec for the  $(1\bar{1}\bar{2}\bar{2})$  peak corresponded to a BSF density of  $2 \times 10^5 \text{ cm}^{-1}$ .<sup>14</sup> The dislocation density was evaluated to be  $2.0 \times 10^{10} \text{ cm}^{-2}$  by TEM. Based on the XRD FWHM and using Kurtz's formula,<sup>40</sup> the dislocation density was estimated to be  $3.0 \times 10^{10} \text{ cm}^{-2}$ . The FWHM of semipolar  $(1\bar{1}\bar{2}\bar{2})$  GaN prepared by a two-step growth process was 630 arcsec.<sup>17</sup> By use of a ScN interlayer, the FWHM of semipolar  $(1\bar{1}\bar{2}\bar{2})$  GaN was 432 arcsec, and the BSF density was estimated to be  $6 \times 10^4 \text{ cm}^{-1}$ .<sup>19</sup> The dislocation density was estimated to be  $1.5 \times 10^8 \text{ cm}^{-2}$  by TEM and  $4.0 \times 10^8 \text{ cm}^{-2}$  by XRD FWHM and using Chierchia's formula.<sup>41</sup> Recently, by growth on etched trenches of r-sapphire, the crystalline quality was improved with an FWHM of 200 arcsec.<sup>42</sup> In this study, the FWHM of the  $(1\bar{1}\bar{2}\bar{2})$  peaks are as small as 180 and 90 arcsec for samples "A2" and "B2", respectively. Correspondingly, the BSF density is estimated to be  $2 \times 10^4 \text{ cm}^{-1}$  for sample "A2" and  $8 \times 10^3 \text{ cm}^{-1}$  for sample "B2". By use of Chierchia's formula, the dislocation density is roughly estimated to be  $1.5 \times 10^8 \text{ cm}^{-2}$  for sample "A2" and  $8.0 \times 10^7 \text{ cm}^{-2}$  for sample "B2".<sup>41</sup> The dislocation density of

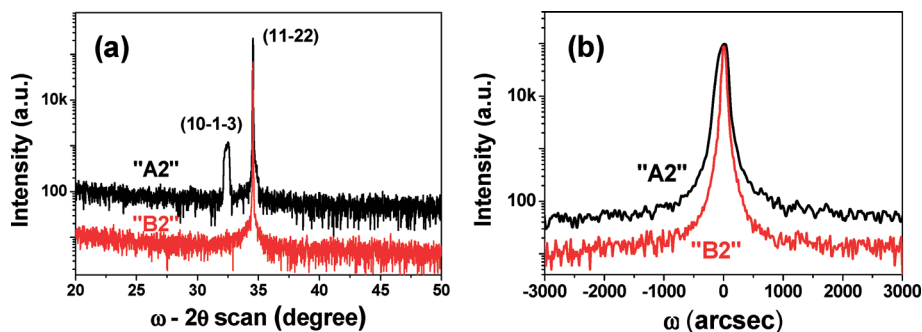


Fig. 8 (a) XRD  $\omega$ - $2\theta$  scans of samples "A2" and "B2". (b) XRD  $\omega$  scans of the (11 $\bar{2}$ 2) peaks from samples "A2" and "B2" with the incident beam direction aligned to  $[\bar{1}\bar{1}23]$ .

sample "B2" was also investigated by TEM and is shown in Fig. 9. In the cross-sectional TEM image view along the  $[\bar{1}100]$  zone axis using  $g = (11\bar{2}0)$ , both a and a + c type dislocations are visible, which are indicated by yellow arrows in Fig. 9a. The dislocation density derived from Fig. 9a is  $\sim 1.2 \times 10^8 \text{ cm}^{-2}$ . The diffraction pattern in Fig. 9b further demonstrates that high-quality semipolar (11 $\bar{2}$ 2) GaN film has been obtained. These results suggest that the *in situ* AISG method may significantly reduce defect density.

Fig. 10 shows the Micro-Raman spectra with clearly visible  $E_2^H$ ,  $A_1(\text{TO})$ , and  $E_1(\text{LO})$  phonon peaks from samples "A2" and "B2". In previous studies, the best FWHM of the  $E_2^H$  peaks was  $3.9 \text{ cm}^{-1}$  for polar *c*-plane GaN and  $3.5 \text{ cm}^{-1}$  for nonpolar *a*-plane GaN.<sup>43,44</sup> Limited by the resolution of the Raman spectroscopy employed in this study and for semipolar (11 $\bar{2}$ 2) GaN, the FWHM of the  $E_2^H$  peaks is relatively broad and estimated as  $12.1$  and  $9.4 \text{ cm}^{-1}$  for samples "A2" and "B2", respectively. The phonon lifetime  $\tau$  is evaluated to be  $0.44 \text{ ps}$  for sample "A2" and  $0.56 \text{ ps}$  for sample "B2", *via* an energy-time uncertainty relation  $\tau = \hbar/\Delta E$ , where  $\hbar = 5.3 \times 10^{-12} \text{ cm}^{-1} \text{ s}$  and  $\Delta E$  is the FWHM in units of  $\text{cm}^{-1}$ .<sup>44</sup> In comparison with  $567.6 \text{ cm}^{-1}$  for strain-free GaN,<sup>45</sup> the  $E_2^H$  peaks of A2 and B2 are located at  $567.7$  and  $568.5 \text{ cm}^{-1}$  with a red shift of  $0.1$  and  $0.9 \text{ cm}^{-1}$ , respectively. The in-plane biaxial residual strain  $\sigma$  can be estimated from  $\sigma = \Delta\omega/K$ , where  $\Delta\omega$  is the peak shift and  $K$  is the linear strain coefficient ( $\sim 4.2 \text{ cm}^{-1} \text{ GPa}^{-1}$ ), to be about  $0.02$  and  $0.21 \text{ GPa}$  in samples "A2" and "B2", respec-

tively. Very small residual compressive strain was left in both samples. The observation of the  $E_1(\text{LO})$  peak at  $740 \text{ cm}^{-1}$  for both samples indicates that almost strain-free high-quality semipolar (11 $\bar{2}$ 2) GaN films were obtained.<sup>46</sup> While the residual strain in sample "B2" is a little bit higher than that in sample "A2", the defect density in sample "B2" is less than that in sample "A2", leading to a more intense and narrower  $E_1(\text{LO})$  peak from sample "B2". Accordingly, high-quality almost strain-free semipolar (11 $\bar{2}$ 2) GaN was obtained by *in situ* AISG, as was consistent with the SEM and XRD results.

Fig. 11 shows the 300 K PL spectra of samples "A2" and "B2". For semipolar GaN on sapphire, the emission peak is in general weak and dominated by defect-related (*e.g.* BSF) emission.<sup>47,48</sup> The peak energies of band-edge emission (BE) "p1", BSF emission "p2", and prismatic SF (PSF) and partial dislocation (PD) emission "p3" measured at 300 K are about  $3.41$ ,  $3.36$ , and  $3.24 \text{ eV}$ , respectively. In Fig. 11 an intense emission peak at  $\sim 3.40 \text{ eV}$  was observed for sample "B2", which is about 4 times stronger than that of sample "A2". Furthermore, the BE intensity ("p1") is much stronger than the intensity of the BSF ("p2"), PSF and PD ("p3") emissions, which suggests that high-quality semipolar (11 $\bar{2}$ 2) GaN films were obtained by *in situ* AISG.

Fig. 12 shows the SEM, panchromatic and  $364 \text{ nm}$  ( $\sim 3.41 \text{ eV}$ ) monochromatic CL images measured at 300 K for samples "A2" and "B2". A ridge-like surface morphology was observed for both samples. Some bright spots in the

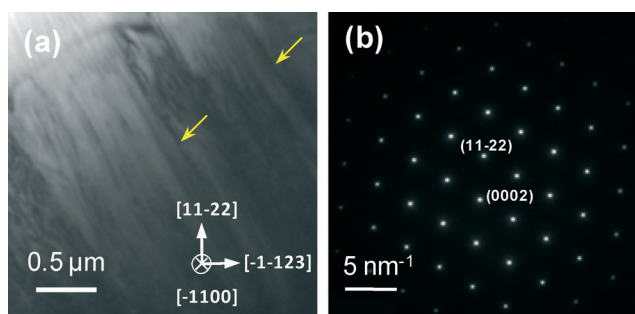


Fig. 9 (a) Cross-sectional TEM images of sample "B2" taken close to the  $[\bar{1}100]$  zone axis with  $g = (11\bar{2}0)$ . The yellow arrows indicate threading dislocations. (b) Selected area diffraction pattern of sample "B2".

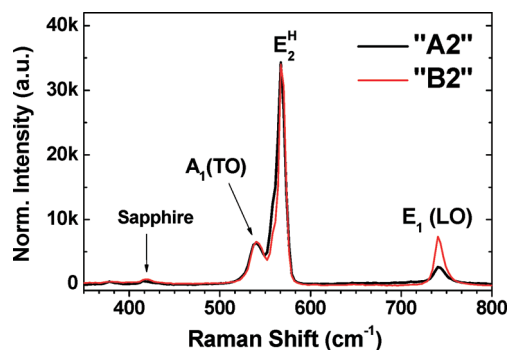


Fig. 10 Micro-Raman spectra of samples "A2" and "B2". The  $E_2^H$ ,  $A_1(\text{TO})$ , and  $E_1(\text{LO})$  phonon peaks are clearly visible.

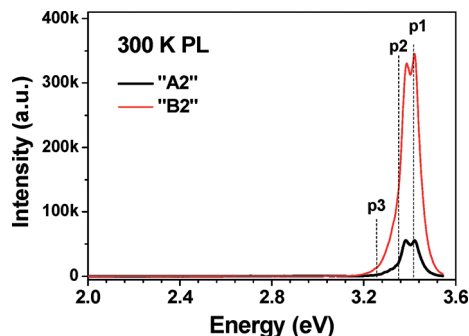


Fig. 11 300 K PL spectra of samples "A2" and "B2".

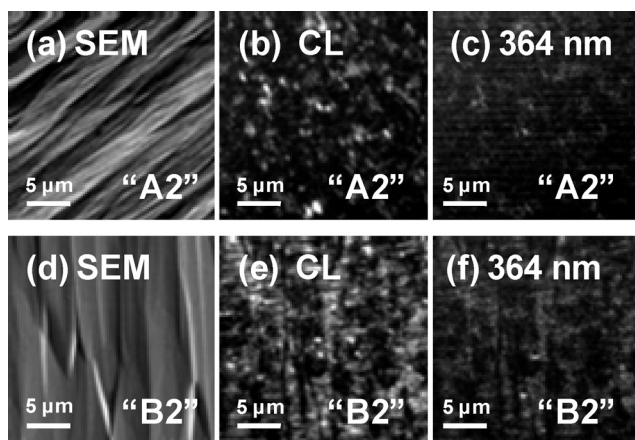


Fig. 12 (a) SEM, (b) panchromatic and (c) 364 nm monochromatic CL images of sample "A2". (d) SEM, (e) panchromatic and (f) 364 nm monochromatic CL images of sample "B2".

panchromatic CL image of sample "A2" with a few weak spots in the 364 nm CL image were observed in Fig. 12b and c, which indicates very weak BE intensity from sample "A2". In comparison, the bright contrast regions in Fig. 12e and f from sample "B2" are broader and brighter than those from sample "A2", which indicates a stronger BE intensity from sample "B2" and a consistency with the growth of large-area high-quality  $+c$  regions by *in situ* AISG.

## Conclusion

Island shaping and its influences on the growth behavior and optical properties of semipolar GaN were studied. *In situ* AISG was developed to form a Ga-rich island surface and enhance the Ga-face facet growth. The  $\{0002\}$  instead of  $\{\bar{1}103\}$  sidewall facets were formed on the islands, which eliminated the formation of the  $\{\bar{1}103\}$  phase during the subsequent layer growth of semipolar GaN. During the island lateral coarsening and coalescence along  $[\bar{1}\bar{1}23]$  the  $+c$  region of the island overlapped the  $-c$  region of a neighboring island, leading to the blocking of SFs formed in the  $-c$  regions. By the use of *in situ* AISG the average striation density estimated from the SEM and AFM images was effectively reduced indicating the reduction of SF density; XRD and TEM studies show that pure semipolar (11 $\bar{2}$ 2) GaN with a basal-plane SF

density of  $\sim 8 \times 10^3 \text{ cm}^{-1}$  and a TDs density of  $\sim 1.2 \times 10^8 \text{ cm}^{-2}$  is obtained; the observation of the narrow  $E_2^H$  peak and intense  $E_1(\text{LO})$  peak in the Raman spectra indicates that almost strain-free high-quality semipolar (11 $\bar{2}$ 2) GaN films were achieved. The luminescence from the semipolar (11 $\bar{2}$ 2) GaN films was significantly enhanced due to the improvement of crystalline quality by *in situ* AISG.

## Acknowledgements

This work was supported by the National Natural Science Foundation of China under Grant No. 11544008, 60876008 and 61076091, and the Fundamental Research Funds for the Central Universities under Grant No. 2012121008.

## References

- 1 A. E. Romanov, T. J. Baker, S. Nakamura and J. S. Speck, *J. Appl. Phys.*, 2006, **100**, 023522.
- 2 J. E. Northrup, *Appl. Phys. Lett.*, 2009, **95**, 133107.
- 3 S. R. Xu, Y. Hao, J. C. Zhang, T. Jiang, L. A. Yang, X. L. Lu and Z. Y. Lin, *Nano Lett.*, 2013, **13**, 3654–3657.
- 4 C. Y. Chang, H. M. Huang, Y. P. Lan, T. C. Lu, L. W. Tu and W. F. Hsieh, *Cryst. Growth Des.*, 2013, **13**, 3098–3102.
- 5 T. R. Kuykendall, M. V. P. Altoe, D. F. Ogletree and S. Aloni, *Nano Lett.*, 2014, **14**, 6767–6773.
- 6 H. Li, L. Geelhaar, H. Riechert and C. Draxl, *Phys. Rev. Lett.*, 2015, **115**, 085503.
- 7 J. W. Hus, C. C. Chen, M. J. Lee, H. H. Liu, J. I. Chyi, M. R. S. Huang, C. P. Liu, T. C. Wei, J. H. He and K. Y. Lai, *Adv. Mater.*, 2015, **27**, 4845–4850.
- 8 Y. Zhao, Q. Yan, C. Y. Huang, S. C. Huang, P. S. Hsu, S. Tanaka, C. C. Pan, Y. Kawaguchi, K. Fujito, C. Van de Walle, J. S. Speck, S. P. DenBaars, S. Nakamura and D. Feezell, *Appl. Phys. Lett.*, 2012, **100**, 201108.
- 9 K. Nishizuka, M. Funato, Y. Kawakami, S. Fujita, Y. Narukawa and T. Mukai, *Appl. Phys. Lett.*, 2004, **85**, 3122–3124.
- 10 B. Imer, F. Wu, J. S. Speck and S. P. DenBaars, *J. Cryst. Growth*, 2007, **306**, 330–338.
- 11 A. Kobayashi, K. Ueno, J. Ohta and H. Fujioka, *Phys. Status Solidi A*, 2011, **208**, 834–837.
- 12 H. Chen, T. Ko, S. Ling, T. Lu, H. Kuo, S. Wang, Y. Wu and L. Chang, *Appl. Phys. Lett.*, 2007, **91**, 021914.
- 13 T. J. Baker, B. A. Haskell, F. Wu, P. T. Fini, J. S. Speck and S. Nakamura, *Jpn. J. Appl. Phys.*, 2005, **44**, L920–L922.
- 14 T. J. Baker, B. A. Haskell, F. Wu, J. S. Speck and S. Nakamura, *Jpn. J. Appl. Phys.*, 2006, **45**, L154–L157.
- 15 T. Wernicke, C. Netzel, M. Weyers and M. Kneissl, *Phys. Status Solidi C*, 2008, **5**, 1815–1817.
- 16 P. Vennegues, Z. Bougrioua and T. Guehne, *Jpn. J. Appl. Phys., Part 1*, 2007, **46**, 4089–4095.
- 17 Q. Sun, B. Leung, C. D. Yerino, Y. Zhang and J. Han, *Appl. Phys. Lett.*, 2009, **95**, 231904.
- 18 J. Jeong, J. Jang, J. Hwang, C. Jung, J. Kim, K. Lee, H. Lim and O. Nam, *J. Cryst. Growth*, 2013, **370**, 114–119.

- 19 M. A. Moram, C. F. Johnston, M. J. Kappers and C. J. Humphreys, *J. Cryst. Growth*, 2009, **311**, 3239–3242.
- 20 S. R. Xu, J. C. Zhang, Y. R. Cao, X. W. Zhou, J. S. Xue, Z. Y. Lin, J. C. Ma, F. Bao and Y. Hao, *Thin Solid Films*, 2012, **520**, 1909–1912.
- 21 C. Q. Chen, J. P. Zhang, J. W. Yang, V. Adivarahan, S. Rai, S. Wu, H. M. Wang, W. H. Sun, M. Su, Z. Gong, E. Kuokstis, M. Gaevski and M. A. Khan, *Jpn. J. Appl. Phys.*, 2003, **42**, L818–L820.
- 22 Z. Bougrioua, M. Laugt, P. Vennegues, I. Cestier, T. Guehne, E. Frayssinet, P. Gibart and M. Leroux, *Phys. Status Solidi A*, 2007, **204**, 282–289.
- 23 X. Ni, U. Ozgur, A. A. Baski, H. Morkoc, L. Zhou, D. J. Smith and C. A. Tran, *Appl. Phys. Lett.*, 2007, **90**, 182109.
- 24 P. de Mierry, N. Kriouche, M. Nemoz and G. Nataf, *Appl. Phys. Lett.*, 2009, **94**, 191903.
- 25 P. Gibart, *Rep. Prog. Phys.*, 2004, **67**, 667–715.
- 26 B. Beaumont, P. Vennegues and P. Gibart, *Phys. Status Solidi B*, 2001, **227**, 1–43.
- 27 T. Bottcher, S. Einfeldt, S. Figge, R. Chierchia, H. Heinke, D. Hommel and J. S. Speck, *Appl. Phys. Lett.*, 2001, **78**, 1976–1978.
- 28 I. Arslan and N. D. Browning, *Phys. Rev. Lett.*, 2003, **91**, 165501.
- 29 L. Lymperakis, J. Neugebauer, M. Albrecht, T. Remmele and H. P. Strunk, *Phys. Rev. Lett.*, 2004, **93**, 196401.
- 30 J. Villain, *Nature*, 1991, **350**, 273–274.
- 31 K. Hiramatsu, K. Nishiyama, A. Motogaito, H. Miyake, Y. Iyechika and T. Maeda, *Phys. Status Solidi A*, 1999, **176**, 535–543.
- 32 Z. L. Fang, J. Y. Kang, W. J. Huang, H. T. Sun, M. Lu, J. F. Kong and W. Z. Shen, *J. Phys. Chem. C*, 2008, **112**, 4925–4931.
- 33 Z. L. Fang, Y. X. Lin and J. Y. Kang, *Appl. Phys. Lett.*, 2011, **98**, 061911.
- 34 A. Lundskog, U. Forsberg, P. O. Holtz and E. Janzen, *Cryst. Growth Des.*, 2012, **12**, 5491–5496.
- 35 J. F. Moulder, W. F. Stickle, P. E. Sobol and K. D. Bomben, *Handbook of X-ray Photoelectron Spectroscopy: A Reference Book of Standard Spectra for Identification and Interpretation of XPS Data*, Physical Electronics, Minnesota, 1995.
- 36 S. Keller, H. R. Li, M. Laurent, Y. L. Hu, N. Pfaff, J. Lu, D. F. Brown, N. A. Fichtenbaum, J. S. Speck, S. P. DenBaars and U. K. Mishra, *Semicond. Sci. Technol.*, 2014, **29**, 113001.
- 37 M. E. Vickers, M. J. Kappers, R. Datta, C. McAleese, T. M. Smeeton, F. D. G. Rayment and C. J. Humphreys, *J. Phys. D: Appl. Phys.*, 2005, **38**, A99–A104.
- 38 B. M. Imer, F. Wu, S. P. DenBaars and J. S. Speck, *Appl. Phys. Lett.*, 2006, **88**, 061908.
- 39 K. C. Kim, M. C. Schmidt, F. Wu, M. B. McLaurin, A. Hirai, S. J. Nakamura, S. P. DenBaars and J. S. Speck, *Appl. Phys. Lett.*, 2008, **93**, 142108.
- 40 A. D. Kurtz, S. A. Kulin and B. L. Averbach, *Phys. Rev.*, 1956, **101**, 1285.
- 41 R. Chierchia, T. Bottcher, H. Heinke, S. Einfeldt, S. Figge and D. Hommel, *J. Appl. Phys.*, 2003, **93**, 8918.
- 42 M. Caliebe, T. Meisch, M. Madel and F. Scholz, *J. Cryst. Growth*, 2015, **414**, 100–104.
- 43 L. Bergman, D. Alexson, P. L. Murphy, R. J. Nemanich, M. Dutta, M. A. Stroschio, C. Balkas, H. Shin and R. F. Davis, *Phys. Rev. B: Condens. Matter Mater. Phys.*, 2007, **59**, 12977.
- 44 H. Y. Gao, F. W. Yan, H. X. Zhang, J. M. Li, J. X. Wang and J. C. Yan, *J. Appl. Phys.*, 2007, **101**, 103533.
- 45 V. Yu. Davydov, Yu. E. Kitaev, I. N. Goncharuk, A. N. Smirnov, J. Graul, O. Semchinova, D. Uffmann, M. B. Smirnov, A. P. Mirgorodsky and R. A. Evarestov, *Phys. Rev. B: Condens. Matter Mater. Phys.*, 1998, **58**, 12899–12906.
- 46 V. Darakchieva, T. Paskova, M. Schubert, H. Arwin, P. P. Paskov, B. Monemar, D. Hommel, M. Heuken, J. Off, F. Scholz, B. A. Haskell, P. T. Fini, J. S. Speck and S. Nakamura, *Phys. Rev. B: Condens. Matter Mater. Phys.*, 2007, **75**, 195217.
- 47 R. Liu, A. Bell, F. A. Ponce, C. Q. Chen, J. W. Yang and M. A. Khan, *Appl. Phys. Lett.*, 2005, **86**, 021908.
- 48 S. Schwaiger, I. Argut, T. Wunderer, R. Rosch, F. Lipski, J. Biskupek, U. Kaiser and F. Scholz, *Appl. Phys. Lett.*, 2010, **96**, 231905.